Electronic Energy Transfer Phenomena in Rare Gases

AHARON GEDANKEN, JOSHUA JORTNER, BARUCH RAZ, AND ABRAHAM SZÖKE
Departments of Chemistry and Physics, Tel-Aviv University, Tel-Aviv, Israel
(Received 25 January 1972)

In this paper we present the results of an experimental study of electronic energy transfer in xenon–argon, krypton–argon, and xenon–krypton gaseous mixtures excited by a pulsed electric discharge. Spectroscopic evidence for electronic energy transfer is based on the decrease in the intensity of the vacuum ultraviolet emission of the excited diatomic homonuclear rare gas molecules in the presence of small amounts (10–1000 ppm) of a foreign rare gas atom, while the visible emission spectrum of the host gas is parctically unmodified under these conditions. The relative contributions of two energy transfer mechanisms involving atom–atom and molecule–atom energy transfer were established by a kinetic analysis of the dependence of the energy transfer efficiency on the host pressure. We have determined the cross sections for energy transfer from the lowest metastable Ar and Kr excited states, and from the lowest excited state of Ar_2^* and Kr_2^* to ground state Xe, and from metastable excited Ar and from Ar_2^* to ground state Kr. The molecule–atom energy transfer process is characterized by large $\sim 10^{-14}$ cm^2 cross sections. A simplified theoretical treatment of excited molecule–ground state atom collisions provides a proper rationalization of these large cross sections in terms of long range dipole–dipole coupling.

I. INTRODUCTION

Vacuum ultraviolet radiation from excited rare gas diatomic molecules is widely utilized as a spectroscopic light source.[1] It was established by Mulliken[2] and by Tanaka *et al.*[3] that homonuclear diatomic rare gas molecules have a large number of bound and repulsive electronically excited Rydberg states. In particular, the lowest excited state is bound, whereas the ground state is repulsive apart from a small van der Waals attraction. Diffuse emission spectra (at moderately low pressures) and continuous emission spectra (at pressures higher than 100 torr) of pure rare gases in the vacuum ultra violet originate from transitions between these two lowest states,[4,5] and can be assigned to bound–continuum transitions, where the atoms at the final state end up with 0.5–1 eV excess kinetic energy.

It is also well known that small amounts of impurities diminish the intensity of the emission continua very efficiently. Atomic and molecular emissions due to the impurities appear instead.[6]

In this work we report the results of a spectroscopic study of the mechanism of radiationless electronic energy transfer between electronically excited rare gas diatomic molecules and rare gas atoms of a different kind. Our key observation is that this energy transfer, caused by collisions between an excited diatomic rare gas molecule and a foreign atom, is a resonant process for a wide range of excitation energies of the acceptor atom. This process can be described by first order time-dependent perturbation theory in terms of a bound–continuum transition of the initially excited diatomic molecule, and a bound–bound transition of the foreign atom. This mechanism is similar to the Forster–Dexter mechanism of energy transfer,[7,8] however, it involves a bound–continuum transition of the energy donor. We find that the electronic energy transfer mechanism can be adequately accounted for in terms of dipole–dipole long range coupling. The large, $\sim 10^{-14}$ cm^2, cross sections for this process, estimated by us, are in qualitative agreement with our experimental results. A new and unexpected emission from the diatomic molecule of the energy acceptor (i.e., xenon or krypton in high pressure argon) even when the partial pressure of the acceptor is as low as 0.1 torr or less, was observed.

A search for new, efficient laser mechanisms in the vacuum ultra violet region is of considerable current interest. Our experimental results make it plausible that rare gas molecule–atom electronic energy transfer phenomena which are characterized by large cross sections, will play an important role in future vacuum uv lasers.

II. EXPERIMENTAL PROCEDURE

The block diagram of the apparatus is presented in Fig. 1. The light source was an improved version of a Tanaka-type lamp (Fig. 2) developed in this laboratory.[9] Pure rare gases and rare gas mixtures were excited by a pulsed electric discharge of 15 kV peak voltage, repetition rate of 1 kHz and an average current of $\sim$70 mA. The discharge tube sealed by a LiF window was attached to the entrance slit of a McPherson 225, 1 m normal incidence vacuum uv monochromator which was equipped with a 1200 lines/mm grating, blazed at 1500 Å. The emission in the spectral range 1100–3000 Å was recorded photoelectrically using an EMI 9514*S* photomultiplier and sodium salicylate converter. Perpendicular to the optic axis of the discharge tube a Jarrel–Ash 250 mm monochromator was used for photoelectric recording of the emission spectrum in the range 3000–8500 Å utilizing photomultipliers with S-5 and S-20 photocathodes.

Matheson research grade gases were used for the preparation of the rare gas mixtures. The discharge tube was baked to 450°C under vacuum and an initial pressure of less than 3×10^{-6} torr was achieved before introduction of the gas mixture. A general purity check of the system and of the gas handling procedure was performed by monitoring the vacuum uv emission

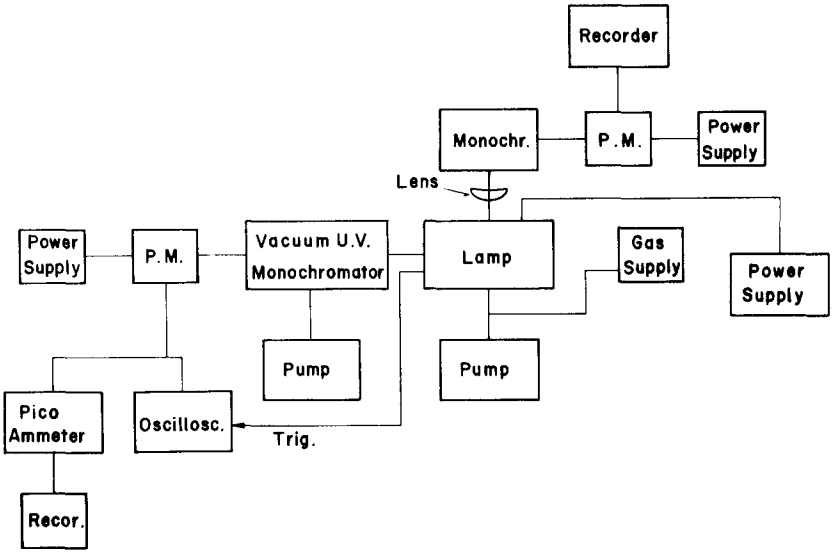

FIG. 1. A schematic representation of the experimental set up.

spectra of the pure rare gases (Fig. 3) at pressures of ~200 torr. We have been able to eliminate almost all "parasitic" atomic emissions resulting from energy transfer to impurity gases except the 1216 Å α-Lyman of hydrogen in argon and the 1470 Å xenon line and the 1656 Å *CI* line in krypton.

III. EXPERIMENTAL RESULTS

A. Vacuum Ultra Violet Emission Spectra

1. Mechanism of Molecular Emission

Two kinds of continua in the vacuum ultraviolet region are emitted by a pure noble gas discharge lamp.[2,3] Their relative intensities are pressure dependent. The so-called "first" structured continuum of the heavier rare gases, starts at the lowest atomic resonance line and extends to the red. It was attributed by Mulliken[2] to transitions from the high vibrational levels of the bound excited $^1\Sigma_u$ molecular state (resulting from the $^3P_1+^1S_0$ atomic states) and of the $^3\Sigma_u$ (originating from the $^3P_2+^1S_0$ atomic states) to the repulsive ground state (see Fig. 4). The broad structureless second continuum is appreciably red shifted relative to the lowest atomic resonance line. It is ascribed to transitions from the vibrationally relaxed levels of the $^1\Sigma_u$ and $^3\Sigma_u$ excited states to the same repulsive ground state (see Fig. 4). The broad emission spectra of pure rare gases excited by an electric discharge at pressures of several hundred torr are identified as originating mainly from the (vibrationally relaxed) second molecular continuum. The high energy side of the emission band may still have some contribution from higher vibrational states of the diatomic molecule, which were not completely relaxed by collisions (see Fig. 4).

The four lowest excited states of the atom involved in the formation of the diatomic molecule belong to the

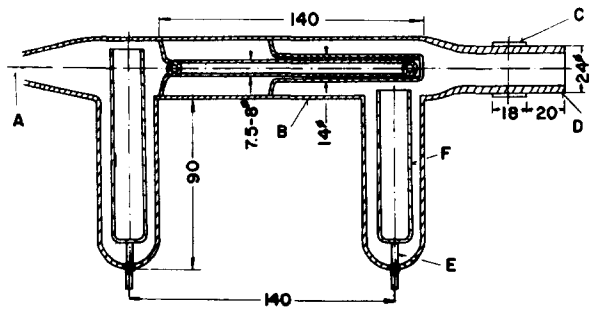

FIG. 2. Discharge tube for emission spectroscopy for rare gases. A, Connection to vacuum system. B, Lamp body made of Pyrex (water cooled). C, Brass sleeve for connection to spectrograph. D, LiF window pressed on to viton "O" ring. E, Tungsten leads. F, Aluminum (99.99%) electrodes.

TABLE I. Radiative and collision induced decay processes in rare gases.

	Ar	Kr	Xe
τ_1 at $p=0$	4.15×10^{-9} [a]	4.38×10^{-9} [b]	3.74×10^{-9} [b]
τ_1 at $p=100$ torr [units of sec]		1.45×10^{-5} [c]	
k_3 torr^{-2}·sec^{-1}	10[d]	44[c]	
k_1 torr^{-1}·sec^{-1}		4400[c]	
τ_2[g] sec	$<3\times10^{-6}$ [f]		$<10\times10^{-6}$ [e]

[a] R. Turner, Phys. Rev. **140,** A426 (1965).
[b] P. G. Wilkinson, Can. J. Phys. **45,** 1715 (1967).
[c] R. Turner, Phys. Rev. **158,** 121 (1967).
[d] D. S. Smith and R. Turner, Can. J. Phys. **41,** 1949 (1963).
[e] C. G. Freeman, M. J. McEwan, R. F. C. Claridge, and L. F. Phillips, Chem. Phys. Letters **10,** 530 (1971).
[f] R. E. Huffman, J. C. Larrbee, and Y. Tanaka, Appl. Opt. **4,** 1581 (1965).

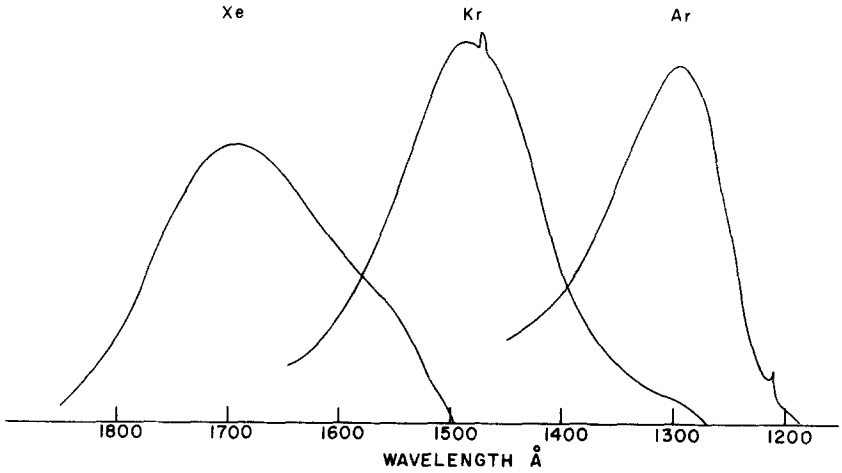

FIG. 3. Vacuum ultraviolet emission spectra of pure rare gases. These spectra represent a faithful reproduction of the recorder output. 1, Argon at 200 torr. The impurity emission line at 1216 Å is due to α Lyman of hydrogen. 2, Krypton at 500 torr. The impurity line at 1470 Å is due to xenon. 3, Xenon at 200 torr. The emission spectra are presented on an arbitrary scale. The actual intensity ratios are 1:5:15 for argon, krypton, and xenon, respectively.

$np^5(n+1)s$ configuration. These states are long lived at high pressures. The $^3P_2$ and $^3P_0$ states are dipole forbidden and the radiation from the $^3P_1$ and $^1P_1$ states to the $^1S_0$ ground state is heavily reabsorbed (imprisoned) in the gas.[10] These long-lived states are populated both by direct excitation from the ground state and by radiative cascades from higher excited atomic states (or ionic states after recombination). An atom in the $^3P_1$ or $^3P_2$ state can form the $^1\Sigma_u$ and $^3\Sigma_u$ molecular states upon collision with an atom of the same kind in the ground state. This molecule formation can occur through binary and ternary collisions,[11] Further collisions relax the newly formed molecule vibrationally. The higher $^3P_0$ and $^1P_1$ states do not form stable molecules.[2]

In the language of the chemist, the description of molecule formation is given above and can be summarized in the following scheme:

$$(^3P_1) \xrightarrow{1/\tau_1} (^1S_0) + h\nu, \qquad \text{(III.1)}$$

$$(^3P_1) + (^1S_0) \xrightarrow{k_1} (^3P_2), \qquad \text{(III.2)}$$

$$(^3P_1) + (^1S_0)[\text{or } 2(^1S_0)] \xrightarrow{k_2} {}^v(^1\Sigma_u^+), \qquad \text{(III.3)}$$

$$(^3P_2) + (^1S_0)[\text{or } 2(^1S_0)] \xrightarrow{k_3} {}^v(^3\Sigma_u^+), \qquad \text{(III.4)}$$

$${}^v(^3\Sigma_u^+)[\text{or } {}^v(^1\Sigma_u^+)] \xrightarrow{k_4} (^3\Sigma_u^+)[\text{or } (^1\Sigma_u^+)], \quad \text{(vibrationally relaxed)} \qquad \text{(III.5)}$$

$${}^v(^3\Sigma_u^+)[\text{or } {}^v(^1\Sigma_u^+)] \xrightarrow{1/\tau_2^v} (^1S_0) + h\nu, \qquad \text{(III.6)}$$

$$(^3\Sigma_u^+)[\text{or } (^1\Sigma_u^+)] \xrightarrow{1/\tau_2} (^1S_0) + h\nu. \qquad \text{(III.7)}$$

The index v denotes a high vibrationally excited diatomic molecule. It should be noted that the atomic lifetime τ_1 is pressure dependent due to radiation trapping. It is also worthwhile noticing that the molecular decay time τ_2^v for $(^3\Sigma_u)$ strongly depends on the internuclear distance.[2] The transition for the $^3\Sigma_u$ state is forbidden at large internuclear separations, i.e., $\tau_2 \gg \tau_2^v$. On the other hand, the decay times for the $^1\Sigma_u$ molecular state will be $\tau_2 \sim \tau_2^v$ for the heavy rare gases, where spin orbit coupling is large. For Ar (and lighter rare gases) it is expected that $\tau_2 < \tau_2^v$. Thus the vibrational relaxation process (III.5), which competes with the radiative decay (III.6), will be more effective in argon than in krypton or xenon. To conclude this brief survey we have displayed in Table I the available kinetic data for the reaction scheme (III).

2. *Spectra*

We have studied the energy transfer in Xe/Kr, Xe/Ar, and Kr/Ar mixtures by introducing controlled

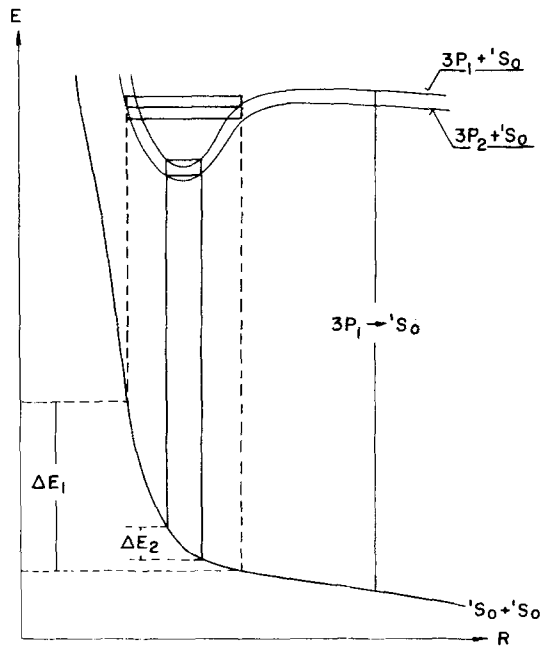

FIG. 4. A schematic representation of the first and the second emission continuum of the diatomic molecules of the rare gases.

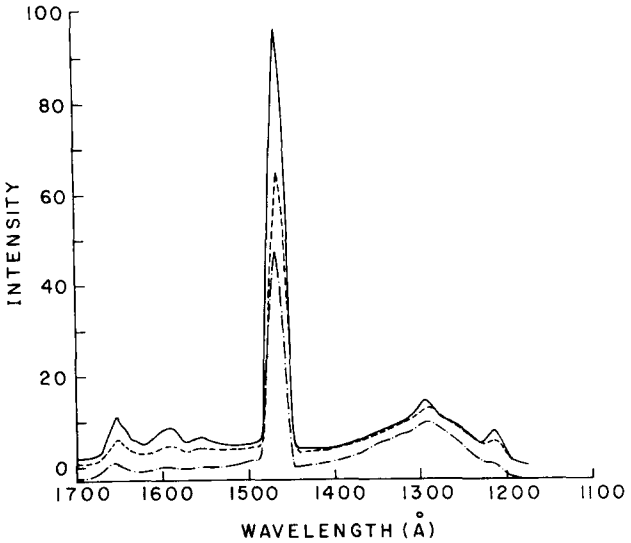

FIG. 5. Low resolution emission spectra of Xe/Ar mixtures at constant xenon number density (of 7.5×10^{18} atoms/cm^3). — 220 torr argon, - - - 320 torr argon, -·- 420 torr argon. This emission spectrum exhibits the Ar_2 molecular emission peaked at 1280 Å, a weak Xe $^1P_1\rightarrow{}^1S_0$ transition at ~1300 Å and a strong Xe $^3P_1\rightarrow{}^1S_0$ transition at ~1470 Å. The lines at 1150 and 1650 Å are due to water and to CI, respectively.

amounts of foreign gases as impurities into host rare gases. (In A/B we denote a mixture consisting of A as a minority additive to B.) In Figs. 5 and 6 we display the emission spectra of argon in the presence of small amounts of xenon. The emission of Xe/Kr mixtures is presented in Figs. 7 and 8 while Fig. 9 exhibits the emission of Kr/Ar mixtures. For spectroscopic studies we have used spectra obtained at moderately high resolution (Figs. 8 and 9) which show self absorption of

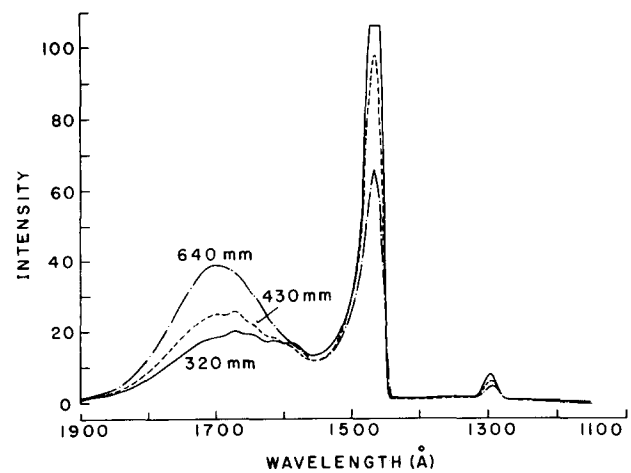

FIG. 6. The low resolution emission spectra of xenon argon mixtures at constant xenon number density (of 7.5×10^{15} atoms/cm^3). The argon pressures are indicated in the figures. At these relatively high xenon concentrations, the prominent features of the spectrum involve the xenon atomic lines at 1296 and 1470 Å and the Xe_2 molecular emission peaked at 1700 Å. Note the absence of the emission peak due to Ar_2 molecule.

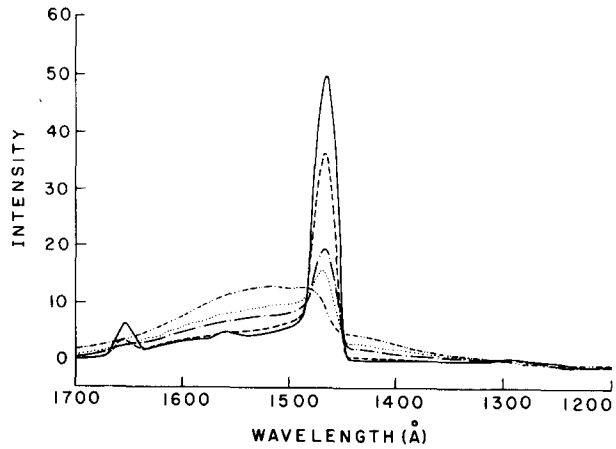

FIG. 7. Low resolution (resolution 25 Å) emission spectra of Xe/Kr. — 70 torr krypton, - - - 130 torr krypton, -·- 230 torr krypton, ··· 320 torr krypton, -···- 460 torr krypton. The spectra are taken at a constant xenon number density of 7.5×10^{-15} atoms/cm^3. The main features of the spectrum involve the xenon $^3P_1\rightarrow{}^1S_0$ emission superimposed on a broad continuum which is attributed to a diatomic molecule containing krypton. Note the absence of the emission at 1296 Å due to $^1P_1\rightarrow{}^1S_0$ xenon atomic transition. The line at 1650 Å is due to CI emission.

the atomic line. For the determination of energy transfer cross sections low resolution spectra (Figs. 5–7 and 9) were used. The important features of these spectra are:

(a) Small amounts of a foreign rare gas (i.e., 0.001–0.1% Xe in Ar or Kr and Kr in Ar) act as a very efficient electronic energy acceptor. This leads to a gradual disappearance of the host's molecular continuum and to the appearance of the resonance atomic emission of the guest atom. Self-absorption (Fig. 8) of the narrow atomic emission atom line demonstrates that they correspond to the atomic resonance emission of the minority constituent.

(b) The Xe/Kr (Figs. 7 and 8) exhibit only the 1470 Å $^3P_1\rightarrow{}^1S_0$ emission whereas the higher energy $^1P_1\rightarrow{}^1S_0$ emission is absent.

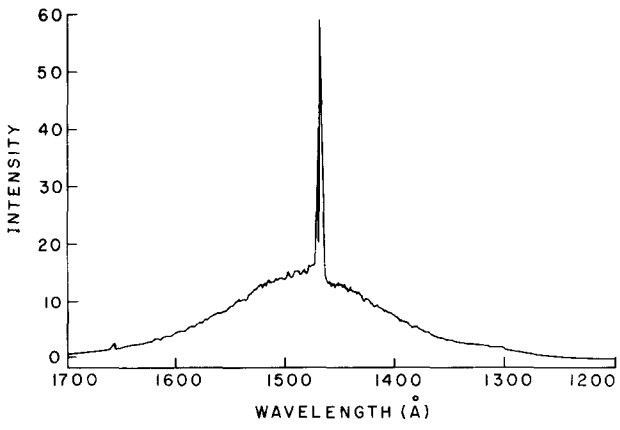

FIG. 8. Medium resolution (0.6 Å) emission spectrum of Xe/Kr exhibiting the self-absorption effect on the xenon 1470 Å line. Xe density is 6×10^{15} atoms/cm^3, the total pressure is 330 torr.

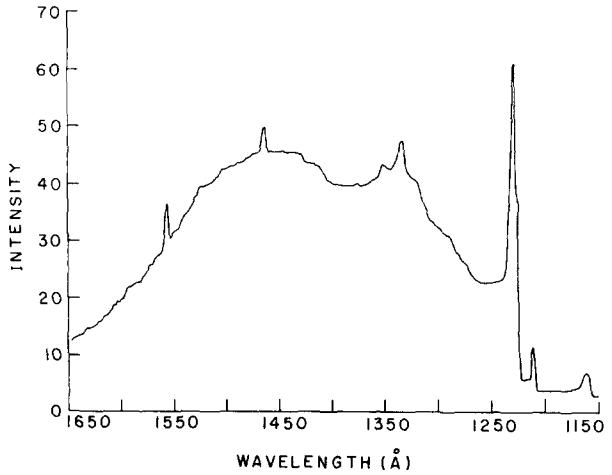

FIG. 9. Low resolution emission spectrum of Kr/Ar mixtures: 1.2×10^{16} atoms/cm^3 Kr, at the total pressure of 220 torr exhibiting the Kr_2 molecular continuum peaked at 1470 Å and the krypton 1240 Å ($^3P_1\rightarrow{}^1S_0$) and 1160 Å ($^1P_1\rightarrow S_0$) atomic transition. The line at 1216 Å corresponds to α Lyman. The 1470 Å line is due to Xe impurity, the 1550 Å originates from H_2O impurity. We were unable to identify the (presumably parasitic) emission at ~1350 Å.

(c) The Kr/Ar mixtures (Fig. 9) reveal prominently the 1240 Å emission line corresponding to the $^3P_1\rightarrow{}^1S_0$ Kr atomic transition and also the Kr 1170 Å line which is due to the $^1P_1\rightarrow{}^1S_0$ transition.

(d) The Xe/Ar mixtures (Figs. 5 and 6) reveal both the 1296 Å ($^1P_1\rightarrow{}^1S_0$) and the 1470 Å ($^3P_1\rightarrow{}^1S_0$) atomic emissions. In the relatively high xenon impurity concentration range employed in the present work, the 1470 Å line is dominant. Very recent studies employing excitation by α particles have demonstrated that with 5 ppm Xe in Ar, about 90% of the atomic emission intensity is due to the 1296 Å ($^1P_1\rightarrow{}^1S_0$) transition.[12] From these results we thus conclude that the 1470 Å Xe emission in the system involves a secondary process which depends upon the xenon concentration. Energy transfer from $Ar_2(^3\Sigma_u$ or $^1\Sigma_u)$ to the xenon atom populates mainly the Xe ($^1P_1$) state.

(e) While in a pure gas the emission from the second molecular continuum is observed only at high (>50 torr) pressures,[13] we were able to observe this second molecular continuum of xenon at low partial pressures (lower than 1 torr) of these guests in high pressure argon host.

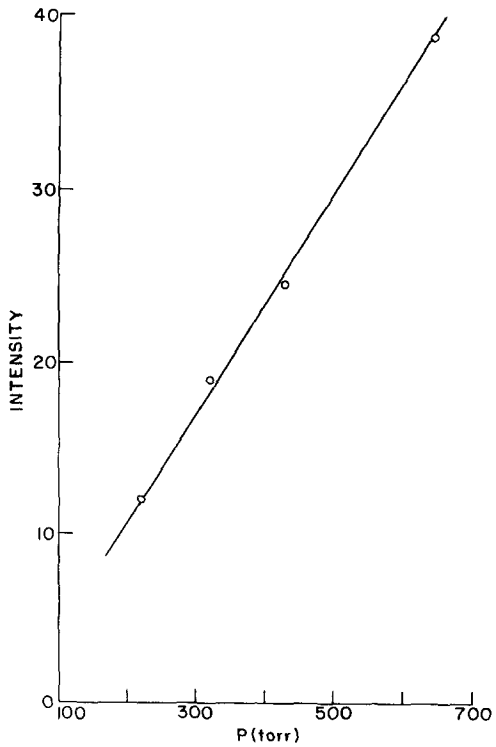

FIG. 10. The dependence of the relative intensity of the Xe_2 emission in Xe/Ar (xenon number density 7.5×10^{15} atom/cm^3) on the argon pressure.

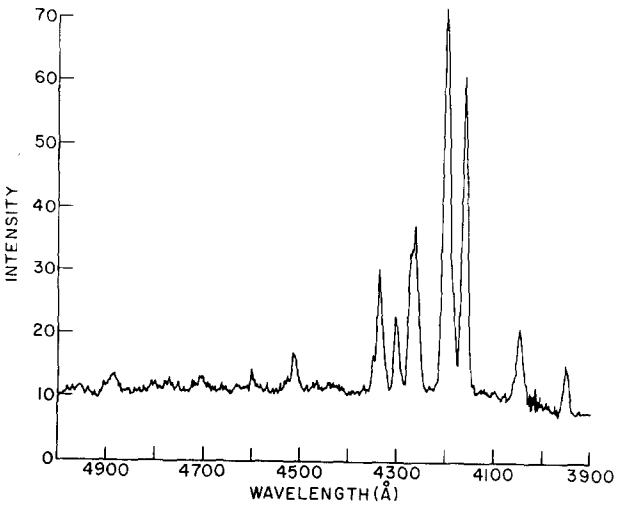

FIG. 11. A sample of the visible emission spectrum of pure argon at 200 torr pressure.

It is apparent from the results displayed in Figs. 5, 6, and 9 that the formation of the diatomic excited molecule consisting of the guest atoms depends both on the guest and on the host partial pressure (Fig. 10). This electronic energy transferred to the guest atom is stored in a metastable state ($^3P_2$) of this atom. This state, whose formation is enhanced by the host pressure, leads subsequently to the formation of the $^3\Sigma_u$ molecular state of the minority component.

B. Visible and Near uv Emission Spectra

The visible and near uv spectrum of a rare gas discharge tube is due to cascades from higher excited states to the lower excited states of the rare gas atoms or molecules. We have recorded the emission spectra of Xe/Ar, Kr/Ar, and of Xe/Kr mixtures in an attempt to establish the role of direct excitation of the foreign

atom. In particular, it is important to establish experimentally the concentration range of Xe and Kr where these direct excitation effects are negligible.

The relative extent of energy transfer from excited atomic states of the host atoms to the guest atoms can be also estimated. It has been experimentally established that some mestable excited atomic states (e.g., Hg^3P_0) have large cross sections for resonant electronic energy transfer.[14] In our system this atomic energy transfer mechanism may effectively compete with energy transfer from the diatomic rare gas molecule to the foreign atom.

In Fig. 11 we present the visible emission spectrum of pure Ar at a pressure of 200 torr. All the observed lines can be assigned to atomic transitions of argon.[15] No bands assignable to transitions between Ar_2 excited molecular states have been observed at this pressure. The prominent transitions in the monitored spectral region are the atomic cascades to Ar ($4s$) states. In Fig. 12 we display the spectrum of 0.1% Xe in Ar. The intensity of the argon spectrum is practically unchanged, while additional xenon lines of comparable intensity appear. The observed additional lines are identified as due to transitions from $6p$ and $7p$ states to $6s$ excited states of xenon.[15] They result from cascades originating from the $9d$ ($J=1$ and $J=2$) xenon atomic levels which coincide well with the $^1P_1$ state of argon. The most prominent feature of these results involves the comparison of the visible and the vacuum ultraviolet emission spectra of rare gas mixtures. While the Ar host visible emission spectrum is practically unmodified in the presence of ~0.1% xenon impurity, the vacuum ultraviolet emission spectrum of this mixture exhibits the complete disappearance of the Ar_2 molecular emission. Thus the changes in the vacuum ultraviolet emission spectra reported in Sec. IIIa can be safely assigned to energy transfer from the host gas to the minority atom and the effects of direct excitation of the minority atom (at low concentrations <1000 ppm) can be neglected.

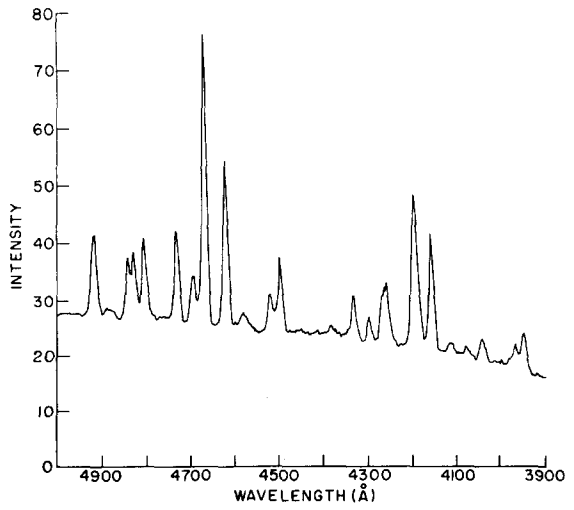

FIG. 12. The visible emission spectrum of Xe/Ar (argon 200 torr, xenon 0.1%) scanned over the same region as in Fig. 11.

TABLE II. Coincidence of atomic states of rare gas atoms[a] (energies in cm^{-1}).

Kr	Ar	Xe
		95 499[$^2P_{3/2}(9d)J=1$]
	95 399($^1P_1$)	95 287[$^2P_{3/2}(10p)J=0$]
		95 274[$^2P_{3/2}(9d)J=2$]
	94 553($^3P_0$)	
94 093[$^2P_{2/3}(5p)J=0$]		93 421[$^2P_{3/2}(5f)J=3$]
	93 750($^3P_1$)	
		93 423[$^2P_{3/2}(9s)J=1$]
93 124[$^2P_{3/2}(5p)J=2$]	93 143($^3P_2$)	
85 847($^1P_1$)		85 440[$^2P_{3/2}(7s)J=1$]
85 192($^3P_0$)		85 189[$^2P_{3/2}(7s)J=2$]
80 917($^3P_1$)		80 970[$^2P_{3/2}(5d)J=3$]

[a] Reference 15.

We have performed a qualitative comparison between the emission spectra of Xe/Ar and of Kr/Ar mixtures (at total pressure of ~200 torr) in the impurity concentration region of 50–10^4 ppm. The Kr visible emission intensity in Kr/Ar was approximately linear in the impurity concentration up to 700 ppm. On the other hand, low Xe concentrations (~50 ppm) in Xe/Ar mixtures give rise to an appreciable emission in the visible region, while comparable concentrations of Kr in Kr/Ar mixtures yield a much lower impurity emission. We conclude that in Kr/Ar mixtures the main pumping mechanism responsible for the impurity visible emission involves direct excitation. On the other hand, in Xe/Ar mixtures an additional efficient pumping mechanism of the Xe impurity atom sets in, which involves atom–atom electronic energy transfer. This conclusion is supported by the good coincidence between the $9d$ ($J=1$ and $J=2$) levels of xenon and the $^1P_1$ state of Ar. Such a matching of excited atomic energy levels is absent in the Kr/Ar system.

IV. INTERPRETATION OF THE EXPERIMENTAL DATA

A. Energy Transfer Mechanisms in Rare Gas Mixtures

The vacuum uv spectra of rare gas mixtures presented so far reveal conclusive evidence for the presence of an efficient energy transfer mechanism to the minority atom. The spectra taken in the visible and in the ultra violet regions show that the host atomic cascade spectrum remained unaffected by the addition of up to 0.1% or rare gas impurity. One is thus led to conclude that the energy transfer occurs either from the low excited metastable atomic levels of the donor (denoted by D^m below), or from its electronically excited molec-

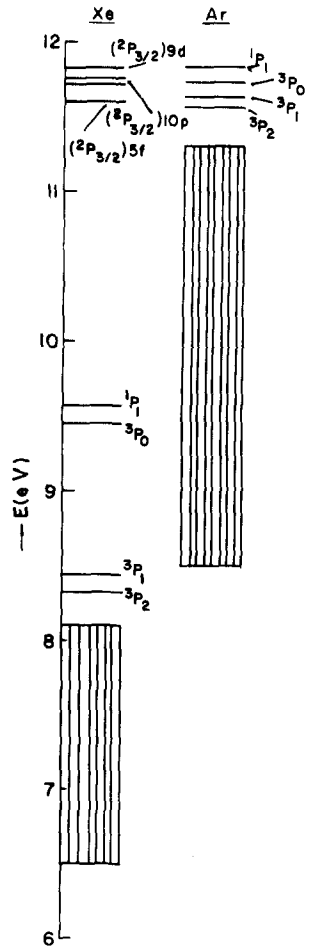

FIG. 13. A schematic representation of the lower atomic and molecular energy levels at the Xe/Ar system. Horizontal lines represent excited atomic levels relative to the ground atomic state. The vertically shaded areas correspond to the energy region spanned by the second molecular continua of these rare gases.

ular $^1\Sigma_u$ and $^3\Sigma_u$ states (denoted by D_2^*). These two energy transfer mechanisms will be now considered.

1. Excited Atom–Ground State Atom Energy Transfer

Higher excited states of noble gas atoms have short (10^{-7} sec–10^{-8} sec) radiative decay times to lower electronic states, therefore they are not expected to act as efficient energy donors at low acceptor concentrations. On the other hand, the lowest excited donor states ($^1P_1$, $^3P_1$) have long (10^{-5} sec–10^{-6} sec) lifetimes,[11] due to radiation imprisonment while the decay of the $^3P_0$ and $^3P_2$ donor states is dipole forbidden. Thus the states $^1P_1$, $^3P_0$, $^3P_1$, $^3P_2$ of the donor can be considered as metastable states. From theoretical arguments it can be shown that a coincidence of the donor and acceptor energy levels of about 200 cm^{-1} or better is necessary for high atom–atom energy transfer cross sections.[15] These energetic coincidences are listed in Table II. From this consideration we expect that the only system in which such coincidence is good enough[16] (energy gap lower than 100 cm^{-1}) is Xe/Ar, which will be characterized by a large $\sim 10^{-14}$ cm^2 cross section. In the Xe/Kr system these cross sections are expected to be of the order of 10^{-15} cm^2.

2. Excited Molecule–Ground State Atom Energy Transfer

This mechanism involves the $^3\Sigma_u$ and $^1\Sigma_u$ molecular states of Ar_2 or Kr_2 and the $Xe(^1S_0)$ on the $Kr(^1S_0)$ states. The molecular states have long ($\sim 10^{-6}$ sec) radiative lifetimes[11] which make the energy transfer feasible. A theoretical analysis of this problem presented in Sec. V, indicates that the cross sections for this process are 10^{-15}–10^{-14} cm^2. The vacuum ultraviolet spectroscopic data obtained herein do not provide evidence for the formation of heteronuclear rare gas diatomic excited molecules, or their participation in the energy transfer processes. The atomic and molecular energy levels pertinent to our considerations appear in Fig. 13 and Table II. The atomic energy levels are well known, while the lowest molecular levels were obtained from the theoretical work of Mulliken[2] and from the experimental work of Tanaka.[3a] It should be noted that the molecular energies refer to vertical Franck–Condon transitions.

According to theoretical arguments which will be presented in Sec. V, we expect that:

(a) Molecule–atom energy transfer is efficient to atomic states which overlap the second molecular continuum of the donor molecule.

(b) Efficient long range molecule–atom energy transfer will occur via dipole–dipole mechanism, so that the resulting electronically excited state will involve an optically allowed excitation of the energy acceptor foreign atom.

(c) Our experimental results (Sec. II.A) indicate that in Xe/Ar, Xe/Kr, and Kr/Ar systems the highest emitting state of the foreign atom involves that allowed state which overlaps with the molecular continuum of the donor molecule, in accord with points (a) and (b).

(d) Atom–atom energy transfer requires near resonance energy level coincidence (within ~ 200 cm^{-1}) between the donor and acceptor excited atomic states.[6] This condition is fulfilled for Xe/Ar and Xe/Ar systems (see Table II) but not for Kr/Ar.

(e) In the Xe/Ar and Xe/Kr systems the atom–atom energy transfer process will occur by a dipole–dipole mechanism (see Table II) and will be thus characterized by a large cross section. On the other hand, in the Kr/Ar system the atom–atom energy transfer will be inefficient both in view of the large energy gap between the donor and the acceptor states and because of unfavorable selection rules.

(f) Atom–atom energy transfer occurs to highly excited states of the energy acceptor. Thus in the Xe/Ar system near resonance transfer takes place from $Ar(^3P_1)$ to $Xe(10s/9p)$ while in the Xe/Kr system energy transfer will occur from $Kr(^3P_1)$ to $Xe(5p^55d)$. The highly Xe atomic states will cascade radiatively to $Xe(^3P_0, ^3P_1, ^3P_2)$ levels.

(g) There is a qualitative difference between the atom–atom and molecule–atom energy transfer mechanisms, as the former results in highly excited states of

the acceptor, while the latter mechanism results in the lowest excited atomic configuration. However, vacuum uv emission studies monitor just the population of the lowest excited configuration of the acceptor atom.

On the basis of these qualitative arguments we cannot assert the relative contribution of the atom–atom and molecule–atom mechanism. The drastic reduction in the molecular continuum intensity in the presence of a foreign gas can be due to efficient molecule–atom energy transfer. However, this effect may originate from atom–atom transfer decreasing the yield of molecule formation [see Eq. (IV.1)]. To settle this crucial point we have to refer to a quantitative analysis of energy transfer cross sections.

B. Energy Transfer Cross Sections

We shall attempt to interpret our experimental data according to the following kinetic scheme:

(i) Metastable donor atoms D^m are produced by radiative cascading or by direct excitation. Following the discussion in Sec. IV.A we shall refer to all the lowest excited states $^3P_0$, $^3P_1$, $^3P_2$ and $^1P_1$ at high D pressure as metastable states.

(ii) The metastable donor atom forms an excited diatomic molecule $D_2^*(^{1,3}\Sigma_u)$ by a three body collision. Utilization of Turner's data[11] indicates that at high D pressures this mechanism dominates over the two body collision mechanism.

(iii) The metastable donor atoms transfer energy to the acceptor atom, A.

(iv) The molecules transfer energy to the acceptor atoms, A.

Thus the simplified kinetic scheme is

$$\begin{aligned} &\overset{k_3}{\longrightarrow} \\ &D^m+A \longrightarrow A^*+D, \\ &\overset{k_1}{\longrightarrow} \\ &D^m+2D \longrightarrow D_2^*+D, \qquad \text{(IV.1)} \\ &\overset{k_2}{\longrightarrow} \\ &D_2^*+A \longrightarrow A^*+2D, \\ &\overset{1/\tau_2}{\longrightarrow} \\ &D_2^* \longrightarrow 2D+h\nu. \qquad \text{(IV.2)} \end{aligned}$$

The steady state concentration of the excited diatomic molecule is

$$[D_2^*]=k_1[D^m][D]^2/(k_2[A]+\tau_2^{-1}). \qquad \text{(IV.3)}$$

Thus the total emission intensity from the second molecular continuum of the donor is given by

$$I(D_2^*)=\tau_2^{-1}[D_2^*]=k_1[D^m][D]^2/\tau_2 k_2[A]+1. \qquad \text{(IV.4)}$$

The total emission intensity $I(A)$ of the acceptor atom (which involves emission both from atomic $A(^1P_1)$ and $A(^3P_1)$ and from molecular $A_2^*(^{3,1}\Sigma_u)$ is given by

$$I(A^*)=k_3[D^m][A]+k_1k_2[D^m][D]^2[A]/(\tau_2k_2[A]+1). \qquad \text{(IV.5)}$$

Thus the experimental intensity ratio is obtained from Eqs. (4) and (5) in the form

$$I(A^*)/I(D_2^*)=k_3\{k_2\tau_2[A]+1\}[A]/k_1[D]^2+k_2[A]\tau_1. \qquad \text{(IV.6)}$$

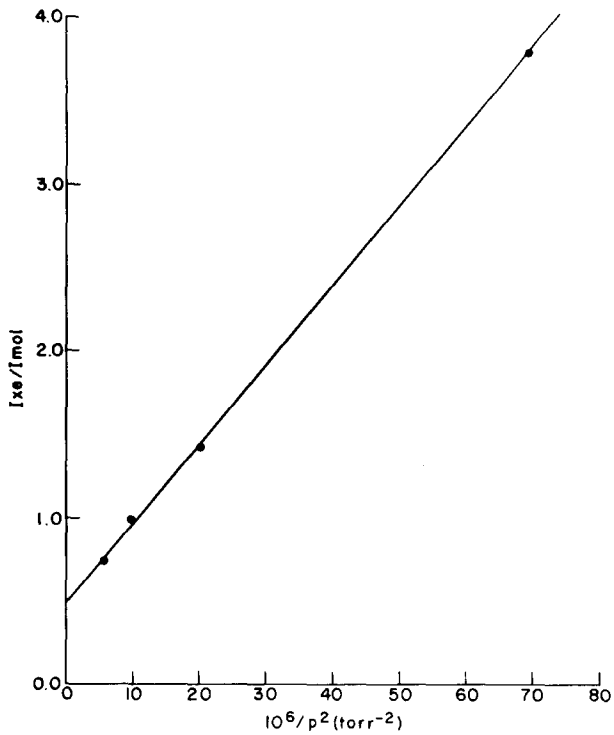

FIG. 14. Determination of the energy transfer cross sections in the Xe/Ar system, according to Eq. (IV.6). The xenon concentration was chosen to be low (7.5×10^{13} atoms/cm^3) to eliminate direct excitation effects. The argon pressure p, was varied in the region 120–640 torr. I_{Xe} represents the total xenon emission (atomic emissions at 1296 and 1470 Å). Under these experimental conditions, the molecular emission of Xe_2 was not observed. I_{mol} represents the emission intensity of the Ar_2 molecule. The intensities were obtained by numerical integration of the emission spectra.

In Figs. 14 and 15 we display our experimental data for the intensity ratio $I(A)/I(D_2^*)$ in the Xe/Ar and Xe/Kr systems obtained at constant [Xe] density plotted according to Relation (IV.6). These experiments were performed at low Xe density (7.5×10^{13} atoms cm^{-3}) so that the role of direct excitation of the minority atom can be neglected. This conclusion is supported by our visible spectra (Sec. III.B) and by the agreement of the experimental data (Figs. 14, 15) with the kinetic analysis [Eq. (IV.6)]. If direct excitation would play a significant role serious deviations from the linear plot of $I(A)/I(D_2^*)$ vs $[D]^{-2}$ are expected.

In order to calculate the rate constants for energy transfer we have utilized the molecular decay time

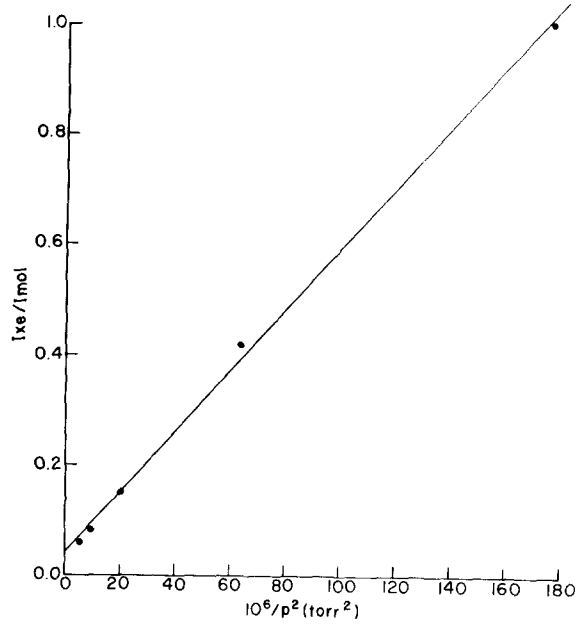

FIG. 15. Determination of energy transfer cross sections in the Xe/Kr system according to Eq. (IV.6). The xenon intensity I_{Xe} was obtained from 1470 Å line while the krypton molecular emission I_{mol} was obtained from the underlying continuum. (The xenon density number 7.5×10^{14} atom/cm^3).

$\tau_2\sim10^{-6}$ sec (see Table I) and Turner's rate[11] $k_1\simeq44$ torr^{-2}·sec^{-1}. The cross sections for atom–atom and molecule–atom energy transfer $\sigma_i=k_i/\langle V\rangle$ $(i=2,\ 3)$ where $\langle V\rangle$ is the relative velocity are displayed in Table III.

The following comments should be made at this point:

(a) In view of our ignorance of the precise values of the radiative decay time τ_2 our estimates of the absolute values of the cross section is reliable within one order of magnitude. However, as our experimental data confirm Relation (6) they provide strong kinetic evidence for the validity of the proposed energy transfer mechanism.

(b) The absolute intensities $I(D_2^*)$ and $I(A^*)$ are proportional to the concentration of the metastable atoms $[D^m]$. It will be worthwhile to determine these concentrations directly by absorption spectroscopy or by electron Raman scattering.

(c) The large $\sigma\sim10^{-13}$–10^{-14} cm^2 cross sections for molecule–atom electronic transfer are consistent with an efficient dipole–dipole long energy transfer mechanism (see Sec. V).

(d) Atom–atom energy transfer in the Kr/Ar system is relatively inefficient relative to the Xe/Ar and to the Xe/Kr systems. This result concurs with the general considerations based on the mismatch of the atomic energy levels in the Kr/Ar system (see Table II).

C. Externally Induced Relaxation in the Xe/Ar System

On the basis of the vacuum uv emission data presented in Sec. III.A we have concluded that in the Xe/Ar system the direct molecule–atom energy transfer process is

$$Ar_2(^{1,3}\Sigma_u)+Xe(^1S_0)\rightarrow 2\,Ar(^1S_0)+Xe(^1P_1). \quad (7)$$

As the Ar_2 $(^{1,3}\Sigma_u)$ second molecular continuum spans the spectral region 1150–1400 Å and peaks at 1280 Å, the population of the Xe $(^1P_1)$ state (located at 1296 Å) is expected to be efficient, while the $Xe(^3P_1)$ state (located at 1497 Å) does not overlap the Ar_2 molecular continuum. Thus, Mechanism (7) is supported both by energy conservation considerations and by experiments at low (~1–10 ppm) Xe concentrations.[12] However, at higher Xe concentrations the population of the $Xe(^3P_1)$ state is predominant as evident from the dominating contribution of the Xe 1496 Å emission in Xe/Ar mixtures (Figs. 5, 6). We have thus to invoke an externally induced relaxation process for the $^1P_1\rightsquigarrow{}^3P_1$ conversion in the Xe/Ar system. The proposed mechanism rests on two physical features of this system: (1) The presence of a $Xe(6p\ ^3D_1)$ excited state located just 84 cm^{-1} above to $Xe(6S\ ^1P_1)$ state.[2] (2) The lengthening of radiative decay time of the $Xe(^1P_1)$ state with increasing Xe concentration due to radiation imprisonment. Thus, in the Xe/Ar system the following $^1P_1\rightsquigarrow{}^3P_1$ conversion mechanism is proposed: (a) The radiative lifetime of the $Xe(^1P_1)$ state varies from 4×10^{-9} sec at $\sim10^{-4}$ torr Xe to $\sim10^{-5}$ sec at 0.1 torr Xe. (b) The radiative decay of $Xe(^1P_1)$ competes with the collisional activation $Xe(^1P_1)+Ar(^1S_0)\rightarrow Xe(^3D_1)+Ar(^1S_0)$. (c) The $Xe(^3D_1)$ decays radiatively to the lower excited $Xe(^3P_2)$ and $Xe(^3P_1)$ states, resulting in the emission from the $Xe(^3P_1)$ state. This mechanism will result in the intensity ratio $I(^1P_1\rightarrow{}^1S_0)/I(^3P_1\rightarrow{}^1S_0)$ for the Xe emission which will depend linearly on the Ar concentration and will exhibit a strong dependence on the Xe concentration due to the lifetime effect. Our data are in qualitative agreement with these expectations.

D. Molecular Emission of the Acceptor

The appearance of the second molecular continuum of Xe and Kr when present at low pressures in Xe/Ar and Kr/Ar mixtures provides a conclusive proof for Turner's idea[11] that rare gas diatomic molecules are produced predominantly from the metastable $^3P_2$ state rather than by ionic mechanisms as proposed by Tanaka.[4] The following mechanism for minority

TABLE III. Cross sections for electronic energy transfer (units 10^{-16} cm^2).

	Donor			
Acceptor	Ar^m	Ar_2^*	Kr^m	Kr_2^*
Xe	2300	2900	2300	320
Kr	59	300		

molecular formation in rare gas mixtures is proposed:

(a) The Kr($^3P_1$) state is produced by direct molecule–atom energy transfer while the Xe($^3P_1$) state is produced by $^3P_1 \rightsquigarrow {}^1P_1$ conversion (see Sec. IV.C).

(b) The lowest allowed $^3P_1$ at "high" Xe and Kr concentrations state is characterized by long radiative lifetimes.

(c) The $^3P_1$ state is deactivated into the long lived $^3P_2$ state by collisions with the Ar gas.

(d) The $^3P_2$ state yields the diatomic homonuclear molecule. In the concentrated region where the guest lifetime is limited by radiation trapping this mechanism exhibits a linear dependence both on the guest and host pressures, in agreement with our qualitative experimental results.

V. A THEORETICAL MODEL FOR MOLECULE–ATOM ENERGY TRANSFER

A basic feature underlying our experimental observations involves the efficient energy transfer from an excited noble gas molecule to an atom of a different kind. In what follows we present some simple theoretical calculations which elucidate the main fetures of this energy transfer process: its large cross section and the relatively weak dependence of this cross section on the electronic energy. The theory of resonant and near resonance electronic energy transfer between atomic states was extensively studied[16] and will not be considered here.

The molecule–atom electronic energy transfer process involves a bound–continuum transition of the energy donor and a bound–bound transition of the energy acceptor. This nonradiative energy transfer process is macroscopically irreversible as the final state of the rare gas diatomic molecule involves a pair of ground state rare gas atoms with large (relative to thermal) kinetic energies. Thus this energy transfer process is analogous to a wide class of molecular radiationless decomposition phenomena such as predissociation,[17] autoionization[18] or Penning ionization.[19]

Within the framework of the Born–Oppenheimer approximation the wavefunction of the donor molecule in the excited electronic state is

$$\varphi_{Mi}{}^e(\mathbf{r}_M, \mathbf{R}_M) = \phi_M{}^e(\mathbf{r}_M, \mathbf{R}_M)\chi_{Mi}{}^e(\mathbf{R}_M), \quad \text{(V.1a)}$$

where $\mathbf{r}_M$ and $\mathbf{R}_M$ denote the electronic and nuclear coordinates, respectively, $\phi_M{}^e$ represents the electronic wavefunction, while $\chi_{Mi}{}^e$ is the vibrational wavefunction in the ith vibrational state, taken for simplicity in the lowest $i=0$ vibrational level. The ground molecular state is given similarly

$$\varphi_{M,E}{}^g(\mathbf{r}_M, R_M) = \phi_M{}^g(\mathbf{r}_M, \mathbf{R}_M)\chi_M{}^g(\mathbf{R}_M, E), \quad \text{(V.1b)}$$

where $\phi_M{}^g$ is the electronic wavefunction of the two ground state atoms. As the ground state is repulsive, $\chi_M{}^g(\mathbf{R}_M, E)$ denotes a volume normalized outgoing wave of the two atoms characterized by the energy E, in the (positive) energy region where the density of states is $P_E \sim E^{1/2}$. The ground $\phi_A{}^g(\mathbf{r}_A)$ and the excited $\phi_A{}^e(\mathbf{r}_A)$ states of the atom acceptor are determined by the atomic electronic coordinates $\mathbf{r}_A$.[16] The collision is now described by the Hamiltonian

$$H = H_M(\mathbf{R}_M, \mathbf{r}_M) + H_A(\mathbf{r}_A) + V(\mathbf{R}, \mathbf{R}_M, \mathbf{r}_M, r_A), \quad \text{(V.2)}$$

where H_M and H_A are the "unperturbed" Hamiltonians for the molecule [expressed in terms of the basis set (V.1)] and for the atom, respectively, while V is the molecule–atom interaction which depends on the atom–molecule spacing $\mathbf{R}$. In the general case of an inelastic (chemically reactive) collision the interaction Hamiltonian has to be expressed in terms of the total Coulomb interaction, and the solution to the problem is very complex. If we anticipate that the lowest order multiple expansion is responsible for long range energy transfer we can write the conventional expression

$$V = \boldsymbol{\mu}_M \cdot \boldsymbol{\mu}_A / R^3 - 3(\boldsymbol{\mu}_M \cdot \mathbf{R})(\boldsymbol{\mu}_M \cdot \mathbf{R})/R^5, \quad \text{(V.3)}$$

where μ_M and μ_A denote the molecular and the atomic transition moment operators, respectively.

Consider first the static approximation whose energy transfer process occurs at a fixed R. The justification for this approximation is that the dipolar interactions (V.3) are of long range and the kinetic energy E in the zero order final state considerably exceeds the thermal energies in the zero order initial state. Now invoking conventional second order time dependent perturbation theory, the transition probability $W_{\text{stat}}(R)$ is given by Fermi's golden rule

$$W_{\text{stat}}(R) = (2\pi/\hbar) \times |[\langle \varphi_{ME}{}^g(\mathbf{R}_M, \mathbf{r}_M)\varphi_A{}^e(\mathbf{r}_A)| \, V \, | \, \varphi_M{}^e(\mathbf{r}_M, \mathbf{R}_M)\varphi_A{}^g(\mathbf{r}_A)\rangle|^2 \otimes \rho_E, \quad \text{(V.4)}$$

where $\langle\ \rangle$ and $(\ )$ denotes integration over electronic and nuclear coordinates, respectively. Making use of Eqs. (V.1) and (V.3), the (V.4) static transition probability can be recast in the approximate form

$$W_{\text{stat}}(R) = (2\pi/h)|(\mathbf{M}_M \cdot \mathbf{M}_A/R^3) - 3(\mathbf{M}_M \cdot \mathbf{R})(\mathbf{M}_A \cdot \mathbf{R})/R^5|^2 F(E), \quad \text{(V.5)}$$

where the atomic transition moment is

$$\mathbf{M}_A = \langle \varphi_A{}^e(\mathbf{r}_A)| \, \boldsymbol{\mu}_A \, | \, \varphi_A{}^g(\mathbf{r}_A)\rangle \quad \text{(V.6)}$$

while the electronic contribution to the molecular transition moment is defined by

$$\mathbf{M}_M(\mathbf{R}_M) = \langle \varphi_M{}^g(\mathbf{r}_M, \mathbf{R}_M)| \, \boldsymbol{\mu}_M \, | \, \varphi_M{}^e(\mathbf{r}_M, \mathbf{R}_M)\rangle. \quad \text{(V.7)}$$

Invoking the Condon approximation we assume that $\mathbf{M}_M(\mathbf{R}_M)$ is a slowly varying function of $\mathbf{R}_M$ around the equilibrium configuration $\mathbf{R}_M$ of the diatomic molecule and we have set in Eq. (V.5) $\mathbf{M}_M = \mathbf{M}_M(\mathbf{R}_M{}^0)$. Finally, the Franck–Condon vibrational overlap factor for the bound–continuum molecular transition is

defined by the relation (taking $i=0$)

$$F(E)=|(\chi_{Mi}{}^{e}(\mathbf{R}_M)|\chi_M{}^{g}(\mathbf{R}_M,E))|^2\rho_E \quad (V.8)$$

which obeys the sum rule for the vibrational overlap integrals

$$\int F(E)dE=1. \quad (V.9)$$

Provided that the Condon approximation for the factorization of the electronic and nuclear contributions to the transition moment is valid the envelope function $F(E)$ can be obtained from the experimental spectroscopic data for the intensity distribution in the second molecular rare gas continua. It is worthwhile to notice at this point that this factorization procedure is adequate for energy transfer from the second but not from the first molecular continuum, as in the latter case the transition moment from high vibrational level of the $^3\Sigma_u$ state may strongly depend on the nuclear coordinate. Finally, it should be stressed that the resonance molecule–atom energy transfer transition probability is characterized by the energy E corresponding to the excited state of the energy acceptor.

In order to gain further insight into the nature of the energy transfer process consider now the branching ratio B, between the radiative decay of the diatomic molecule, characterized by the molecular decay probability, $W_{\rm rad}$, and the nonradiative decay which is characterized by the orientatially averaged probability $\langle\langle W_{\rm stat}\rangle\rangle$, so that

$$B(R)=\langle\langle W_{\rm stat}(R)\rangle\rangle/W_{\rm rad}. \quad (V.10)$$

The total radiative decay probability is

$$W_{\rm rad}=\tfrac{4}{3}(M_M{}^2\omega^3/\hbar c^3)\int F(E)dE$$
$$=\tfrac{4}{3}(M_M{}^2\omega^3/\hbar c^3), \quad (V.11)$$

where we have again invoked the Condon approximation and utilized Eq. (V.9). Making use of (V.10), (V.5), and (V.11), we get

$$B(R)=\tfrac{2}{3}(|M_A|^2c^3/R^6\omega^3)F(E)$$
$$=(1/8\pi^2)(\lambda/R)^3(|M_A|^2/R^3)F(E), \quad (V.12)$$

where λ is the average wavelength of molecular emission and the factor (2/3) in (V.12) originates from spherical averaging. Equation (V.12) demonstrates that the electronic energy transfer rate is proportional to the molecular radiation rate, and also to the atomic radiation rate. This is not surprising as we have applied the dipole approximation for the interaction potential.

It will be helpful at this stage to introduce the quenching radius, R_q, defined by the relation

$$B(R_q)=1 \quad (V.13)$$

so that at the molecule atom spacing $R=R_q$ the radiative molecular decay probabilities are equal. From Eqs. (V.12) and (V.13) we get

$$R_q=[(1/8\pi^2)\lambda^3|M_A|^2F(E)]^{1/6}. \quad (V.14)$$

Some numerical estimates are now in order. For a typical diatomic rare gas molecule–atom pair we set $\lambda\approx1500$ Å, $M_A=1$ D $W_{\rm rad}\approx1/\tau_T\approx10^6$ sec^{-1} and the Franck–Condon (normalized) emission envelope is approximated by a rectangular distribution of a width of 5000 cm^{-1}, i.e., $F(V)=2\times10^{-4}$ cm. Thus for resonance energy transfer (where the excited atomic state effectively overlaps the molecular emission) we get $R_q=30$ Å for the quenching radius. It has to be emphasized that for such large distances the dipole approximation is certain valid. Finally the nonradiative transition probability can be now recast in the useful form

$$\langle\langle W_{\rm stat}(R)\rangle\rangle=(R_q/R)^6W_{\rm rad}\approx8\times10^{14}/(R/\text{Å})^6\ \text{sec}^{-1}, \quad (V.15)$$

where we have again taken $W_{\rm rad}=10^6$ sec^{-1}.

A rough estimate of the energy transfer cross section can be obtained from a dynamic theory adopted from Miller's work on Penning ionization.[19] We shall limit ourselves only to the classical apprximation, whereupon the transition probability P in a collision characterized by an impact parameter b is given by

$$P(b)=1-\exp\left[-\int_{-\infty}^{\infty}dt\Gamma(R)\right]. \quad (V.16)$$

The linewidth parameter in the Born–Oppenheimer approximation is given by $\Gamma(R)=W_{\rm stat}(R)$. Performing the integration over a straight line and ignoring the angular dependence we get

$$P(b)=1-\exp\left[-\int_{-\infty}^{\infty}\frac{W_{\rm rad}R_q{}^6dx}{R^6\langle V\rangle}\right]$$
$$=1-\exp[\tfrac{3}{8}\pi W_{\rm rad}(R_q/b)^6(b/\langle V\rangle)]. \quad (V.17)$$

A dynamic transfer radius R_d can be defined by the condition $P(R_d)=1-e^{-1}$, and we get

$$R_d=R_q(\tfrac{3}{8}\pi W_{\rm rad}R_q/\langle V\rangle)^{1/5}. \quad (V.18)$$

The cross section for energy transfer is

$$\sigma=\pi R_d{}^2 \quad (V.19)$$

and making use of Eq. (V.14) we have

$$\sigma=(\pi\tfrac{8}{15}\pi\lambda^3|M_A{}^2|F(E)/\langle V\rangle)^{2/5}. \quad (V.20)$$

Making use of $R_q=30$ Å, $W_{\rm rad}=10^6$ sec^{-1}, and $v=2\times10^4$ cm sec^{-1} we get, from (V.20), $R_d=0.1$, $R_q=3$ Å and $\sigma=3\times10^{-15}$ cm.

From the results we conclude that:

(a) Molecule atom electronic energy transfer is characterized by large cross sections in qualitative agreement with our experimental data.

(b) Dipole dipole long range transfer mechanism is favored for large transition moments of the acceptor (i.e., large M_A) and of the molecular donor (i.e., large M_M and large $W_{\rm rad}$). This mechanism obviously leads

to energy transfer to the optically allowed atomic excited states.

(c) The transfer cross section will exhibit only a weak temperature dependence due to the term $\langle V\rangle^{-2/5}$ in (V.20).

(d) The energy transfer cross section is nonvanishing only in the range where the allowed atomic transition energy E overlaps the molecular emission function $F(E)$. In this energy range σ exhibits a weak energy dependence of the form $[F(E)]^{2/5}$.

The theoretical estimates of the molecule–atom electronic energy transfer cross sections σ (estimated) 10^{-15}–10^{-14} cm^2 are lower by about 1 order of magnitude than the experimental values σ (experimental 10^{-14}–10^{-13} cm^2. This discrepancy should not worry us in view of the approximate treatment of the collision process employed herein. To quote an analogous precedent consider the well known case of resonance dipole–dipole atomic energy transfer.[16] The application of a semiclassical treatment of the collision process yields[16] for the cross section $\sigma_A\sim\mu_A^2/3\hbar\langle V\rangle$, and taking $\mu_A\sim 1$ D for the atomic transition moment results in $\sigma_A\sim 2.5\times10^{-14}$ cm^2 at $T=300$°K. A more elaborate treatment results in $\sigma_A\sim10^{-12}$ cm^2, the discrepancy between the approximate and exact treatments being again about one order of magnitude. We expect, however, that the approximate treatment of molecule–atom energy transfer presented herein elucidates the gross features of this interesting process.

VI. LASER APPLICATIONS

Lassers in the vacuum uv region of the spectrum are few and far apart. It is only very recently that population inversion has been obtained in gaseous H_2, CO [20,21] and indication of population inversion of Xe has been shown in the condensed phase.[22] In these lasers direct excitation by electrons gives transient inversion. CW lasers go as far as 3250 Å in the He–Cd$^+$ system.[23] Our studies were undertaken partly in search of pumping mechanisms for lasers in the short wave regions. We have seen in previous sections that energy transfer from high pressure noble gases is efficient. In this section some possible laser applications will be pointed out. Most of the ideas are not new, but we believe their execution becomes more feasible by our results.

We will start with a survey of lasers relevant to our discussions. More details can be found in a recent review by Rhodes and Szöke.[24] The first gas laser, the He–Ne system, is based on energy transfer from metastable He atoms. The cross section for transfer is $\sigma=4\times10^{-17}$ cm^2 and only a small part of the energy is utilized.[24] The N_2–CO_2 system, a very efficient one, is based on a similar mechanism. It was proposed by Parks and Javan[25] some years ago that excited noble gas molecules have a population inversion even at very low production rates. The mechanism, parts of which were mentioned above, is the following: At the equilibrium intermolecular distance of the molecule ground state, atoms possess large potential energy. In an electromagnetic transition the internuclear distance does not change, therefore the concentration of absorbers is very low. In order to get laser action the gain has to be at least a few percent per meter; thus a large concentration, n, of emitters is needed

$$n=12\pi^3(g\lambda^{-2})(\Delta\omega t)]=2\times10^{17}/\text{cm}^3.$$

In order to achieve this, the pumping power P, must be large

$$P=(1-e^{-T/\tau})^{-1}(6\pi/2)(\hbar w^3/c^2)g\Delta w=2.5\times10^6\ \text{W/cm}^3$$

for a $T=10^{-7}$ sec pulse. The total energy $\epsilon=PT=2.5\times10^{-1}$ J is not high, in fact, the vacuum uv lasers of Hodgson and Shipman[21] do have appropriate power levels. Another system which is relevant to our discussion is the He–Cd$^+$ and related systems. In these systems Penning collisions which have a large cross section ($\sigma=4\times10^{-15}$ cm^2) populate the upper laser levels. As we pointed out earlier, the transfer of energy from noble gas molecules has similarities to this process in that it is also resonant and has a large cross section which depends on energy only mildly.

In some high power, high pressure, pulsed noble gas lasers energy transfer from molecules may be of importance. The example for our discussion is the He:Xe system.[24] These lasers have inversion mechanisms which are similar to that of the He:Ne system—an upper level of long lifetime is populated preferentially, it becomes inverted with respect to another lower lying state which as a shorter lifetime. As cascades play a significant part in the inversion process it should be quite insensitive to the exact resonance condition in the inversion. Energy transfer from molecules and from metastable atoms should provide an efficient pumping mechanism at high host-gas pressures. At high pressures the transfer can be very fast, therefore, in a pulsed system re-excitation from metastable levels can be reduced, thus an important bottleneck of laser action eliminated.

Some significant new high pressure laser systems can be expected because of the similarity between Penning collisions and the energy transfer from noble gas molecules. It is interesting to note that the final state in a collision of the type $He_2^*+Cd\rightarrow He+He+Cd^{+*}+e$ is a continuum state with four bodies. It has a phase space distribution which is significantly different from that which appears in the usual Penning collision ($He^*+Cd\rightarrow He+Cd^{**}+e$). Also the cross section may be larger because some molecular transitions are dipole allowed. The nature of the energy transfer from a molecule is such that it may populate excited states of excited molecules also very efficiently. In preliminary experiments in a Ne:H_2 mixture very efficient excitation transfer was observed by us and both atomic and molecular emission lines have been seen in great profusion.

The relative merits of a direct excitation H_2 laser and one operated through energy transfer cannot be evaluated at the present time.

There are some new laser systems possible using resonant energy transfer from molecules. Consider the collision $Ar_2^*Xe \rightarrow Ar+Ar+Xe^*$ discussed at length in Secs. IV and V and its reverse collision. The principle of detailed balance apples, therefore, the collision cross sections are related by some phase space factor. In fact, the population of a pair of Ar atoms with the required kinetic energy KE is $[Ar]^2 \exp[-KE/kT]$, therefore the reverse collision rate in a gas at a low kinetic temperature is negligible. In fact it is exactly $\exp[-KE/kT]$ times the rate which would follow from considerations of phase space alone. This happens essentially because the argon atoms which fly apart with a high kinetic energy lose their energy to the surrounding gas before they collide again. It is thus possible to invert the population of the acceptor atom with respect to the ground state. As an example, two sets of levels in Xe will be considered. The transition from $^3P_1$ to $^1S_0$ the ground state is dipole allowed, it has a lifetime of $\tau=2\times10^{-9}$ sec. In a noninverted gas this lifetime is considerably lengthened by imprisonment of the resonance radiation. When inversion approaches, the imprisonment is absent, though if the excited region is in the shape of a long filament, part of the imprisonment can still be present. The rate equation for excited Xe can be written

$$d[Xe^*]/dt=-[Xe^*]/\tau+[Ar_2^*][Xe]\sigma\langle V\rangle,$$

where, as in Sec. IV, $[Xe^*]$, $[Xe]$, $[Ar_2^*]$ represent the concentrations of excited Xe, ground state Xe, and molecular Ar, respectively, $\langle V\rangle$ is the mean relative velocity, τ is the lifetime of excited Xe, and σ is the cross section for energy transfer from Ar_2^* to Xe. The condition for inversion in steady state (i.e., for excitation pulses longer than τ) is $[Xe^*]/[Xe]>1$. It can be written as

$$[Ar_2^*]>1/V\sigma\tau=1.5\times10^{18}\ \text{cm}^{-3}.$$

This number is quite high, in fact it gives a gain of ~2/m on the Ar_2^* transition itself. Still this number of Ar molecules is achievable in a high pressure gas discharge. The formation rate of Ar molecules is given by Turner[11] as $R=\alpha p^2$, where $\alpha=10\ \text{sec}^{-1}\cdot\text{torr}^{-2}$. Thus in a discharge of 1000 torr the rate of formation of molecules is $R=10^7\ \text{sec}^{-1}$. This rate will probably be limited in practice by the radiative cascades of excited Ar states. The gain of the Xe transition is given by

$$g=\tfrac{2}{3}([Xe^*]-[Xe])\lambda^2/(2\pi)^3(\Delta w\tau),$$

where Δw is the linewidth, τ is the lifetime of the upper level, λ is the wavelength of the transition, $[Xe^*]-[Xe]$ is the population inversion. Note that $\Delta w\tau$ is greater than one from the uncertainty principle. We assume that $\Delta w\tau=10^2$ for Xe, but for a Xe_2^* molecule it is $\Delta w\tau=10^{15}\times10^{-6}=10^9$. Assuming an inversion $[Xe^*]-[Xe]=3\times10^{15}/\text{cm}^3$ and that the Xe pressure is $p=10^{16}/\text{cm}^3=1/3$ torr, we get a gain $g=16$/cm. Such a laser should work easily without mirrors. The pulse energy needed, assuming an efficiency $\eta=10\%$ is $\epsilon=[Ar_2^*]\hbar w/\eta=2J$. There are some known problems associated with this inversion scheme.[24] There are two competing channels which populate the Xe levels; one goes through the Ar_2^* molecule and it gives rise to total inversion, as discussed above, the other is transfer from metastable Ar atoms. The latter mechanism does not necessarily lead to complete inversion, it depends on the relative positions of the donor (Ar metastable) and acceptor levels. If this latter mechanism is predominant, it can be suppressed by using high pressure Ar. Another possible problem is the excitation of other unwanted Ar and Xe levels, e.g., the formation of Xe molecules though these are not expected to be detrimental.

On the surface, it seems from the above argument that inversion of the metastable $^3P_2$ level of Xe should be much easier. In fact, its lifetime at high Ar pressures is determined by the collisional excitation of $Xe(^3P_2)$ to $Xe(^3P_1)$, where it radiates. There is a range of pressures and discharge energies such that these two levels reach thermal equilibrium and the radiation of $^3P_1$ is still trapped, making its effective lifetime long. Nevertheless, it is difficult to predict a priori what will happen. The excitation of metastables by electrons and by ions can be large. Xe ions may be formed etc. However, it is interesting to note that an inversion of the $^3P_2$ metastables with respect to the ground state can be utilized in an anti-Stokes Raman laser. It has been shown by Javan[26] that Raman laser action is possible in a *non*inverted system on the Stokes component. Similar considerations show that Raman laser action is possible in a system where the population is inverted on the anti-Stokes line and on the stimulated two photon emission. Calculations show that the gain is reasonable.

[1] J. A. R. Samson, *Techniques of Vacuum U. V. Spectroscopy* (Wiley, New York, 1967).
[2] R. S. Mulliken, J. Chem. Phys. **52,** 5170 (1970).
[3] (a) Y. Tanaka and K. Yoshino, J. Chem. Phys. **53,** 2012 (1970). (b) M. C. Castex and N. Damany (private communication).
[4] (a) Y. Tanaka and M. Zelikoff, Phys. Rev. **93,** 933 (1954). (b) Y. Tanaka and M. Zelikoff, J. Opt. Soc. Am. **44,** 254 (1954). (c) Y. Tanaka and A. S. Jursa, *ibid.* **50,** 1118 (1960).
[5] R. C. Michaelson and A. L. Smith, Chem. Phys. Letters **6,** 1 (1970).
[6] For a recent survey of this problem, see: A. Gedanken and B. Raz, Vacuum **21,** 389 (1971).
[7] Th. Forster, Ann. Physik **2,** 55 (1948).
[8] D. L. Dexter, J. Chem. Phys. **21,** 836 (1953).
[9] B. Raz, J. Magen, and J. Jortner, Vacuum **19,** 571 (1969).
[10] (a) T. Holstein, Phys. Rev. **72,** 1212 (1947); (b) **83,** 1159 (1951).
[11] (a) D. S. Smith and R. Turner, Can. J. Phys. **41,** 1949 (1969). (b) R. Turner, Phys. Rev. **140,** A426 (1965); (c) **158,** 121 (1967).
[12] A. Cheshnovsky, B. Raz, and J. Jortner, Proceedings of the

Third International Vacuum Ultraviolet Conference, Tokyo, 1971.
[13] P. G. Wilkinson, Can. J. Phys. **45**, 1715 (1967).
[14] (a) M. W. Zemansky, Phys. Rev. **36**, 919 (1930). (b) M. G. Evans, J. Chem. Phys. **2**, 445 (1934).
[15] C. E. Moore, "Atomic Energy Levels" Natl. Bur. Std. Circ. No. 467, Vol. 3, 1958.
[16] H. S. W. Massey, *Electronic and Ionic Impact Phenomena*, (Oxford U. P., New York, 1971), Vol. 3.
[17] R. A. Harris, J. Chem. Phys. **39**, 978 (1963).
[18] U. Fano, Phys. Rev. **124**, 1866 (1961).
[19] W. H. Miller, J. Chem. Phys. **52**, 3563 (1970).
[20] R. T. Hodgson, Phys. Rev. Letters **25**, 494 (1970); R. W. Waynant, J. D. Shipman, R. C. Elton, and A. W. Ali, Appl. Phys. Letters **17**, 383 (1970).
[21] R. T. Hodgson, J. Chem. Phys. **55**, 5378 (1971).
[22] N. A. Basov, V. A. Danilychev, Yu. M. Popov, and D. D. Khodkevich, ZhETF Pis. Red. **12**, 473 (1970) [JETP Letters **12**, 329 (1970)].
[23] W. T. Silfvast, A. R. Fowles, and B. D. Hopkins, Appl. Phys. Letters **8**, 318 (1966); W. T. Silfcast, *ibid.*, **13**, 169 (1968).
[24] C. K. Rhodes and A. Szöke, in *Laser Handbook*, edited by T. Aveechi and E. Schulz DuBois (North Holland, Amsterdam, 1972).
[25] J. H. Parks and A. Javan (unpublished).
[26] A. Javan, Phys. Rev. **107**, 1579 (1957); reviewed, e.g., in *Quantum Optics*, edited by R. J. Glauber (Academic, New York, 1969).

THE JOURNAL OF CHEMICAL PHYSICS VOLUME 57, NUMBER 8 15 OCTOBER 1972

Circular Dichroism of Oriented Helical Polypeptides: the Alpha-Helix

RICHARD MANDEL AND G. HOLZWARTH
Department of Chemistry and Department of Biophysics, University of Chicago, Chicago, Illinois 60637

(Received 19 May 1972)

The oriented circular dichroism spectrum of an alpha-helical polypeptide in solution is reported between 190 and 250 nm. The linear dichroism, absorption, and unoriented circular dichroism are obtained for the same solvent–polymer system. The four curves are resolved into a single set of bands consistent with the conclusions of exciton theory. It is shown that (1) the rotatory bands of the helix predicted by Moffitt are allowed only for light propagating perpendicular to the helix axis, (2) the additional rotatory strength predicted theoretically by Moffitt, Fitts, and Kirkwood is detectable and is allowed only for light propagating parallel to the helix axis. However, the Moffitt–Fitts–Kirkwood band has only $\frac{1}{4}$ the intensity predicted by strong-coupling exciton theory.

INTRODUCTION

We have measured the oriented circular dichroism (CD) of the polypeptide alpha-helix between 190 and 250 nm. In contrast to measurements on unoriented samples, these experiments yield the individual diagonal components of the rotational strength tensor, and thereby provide a stringent test of the strong-coupling exciton theory for the optical properties of rodlike helical polymers. This theory, originally proposed by Moffitt[1] and by Moffitt, Fitts, and Kirkwood,[2] has been extensively developed by Tinoco and Woody.[3–5] Some aspects of the theory, notably the role of end effects and the proper application of the Born–von Karman boundary condition, have recently been clarified by Ando,[6] Loxsom,[7] Deutsche,[8] and others.[9] All of this theoretical work is now in essential agreement as to predictions for a general helical model. Moreover, the theory has been applied, by detailed numerical calculations, to predict the optical properties of the α-helix.[5,10,11]

Many of the major features of exciton theory have received experimental support by studies upon α-helical polypeptides: Splitting of the $\pi \rightarrow \pi^*$ absorption band has been observed[12]; the polarization of the split components has been verified[13,14]; the major features of the unoriented CD pattern confirm theoretical predictions.[5,15,16] However, no firm experimental evidence has been obtained for the additional CD band θ_H first predicted by Moffitt, Fitts and Kirkwood[2] and all subsequent calculations, although theory predicts the band to be large in the α-helix.[10,11] Indeed, Cassim and Yang[17] recently presented optical rotatory dispersion (ORD) evidence *against* the existence of the band, and Johnson and Tinoco[18] were unable to discern it clearly in a vacuum uv CD study, because of an overlapping CD band at 175 nm. However, earlier oriented ORD curves between 300 and 600 nm by Tinoco and co-workers[5,19] provided indirect evidence for the band and its polarization. The present study takes advantage of the directional nature of the rotational strength tensor to obtain evidence for the θ_H band and to show that the other rotatory bands have the polarization predicted by theory.

In addition to the oriented CD curve, absorption, linear dichroism, and CD are obtained for the same polymer–solvent system. The four spectra are resolved into a self-consistent set of absorption and rotatory bands associated with the $n \rightarrow \pi^*$ and $\pi \rightarrow \pi^*$ transitions. Similar experimental studies of collagen and poly-L-proline will be presented in a succeeding paper.[20]

RESUME OF THEORETICAL PREDICTIONS

Let us outline the first-order predictions of the theory[1–9] for a simple exciton band, following the